DEVELOPMENT OF NOVEL MEMBRANES WITH COMPETITIVE BINDING PROPERTIES FOR THE ARTIFICIAL KIDNEY

Maria Inês Santos
Instituto Superior Técnico, Lisboa, Portugal

October 2022

Abstract

A competitive binding strategy was used to functionalize monophasic hybrid cellulose acetate/silica (CA/SiO_2) membranes with ibuprofen (IBF) to enhance protein-bound uremic toxins (PBUTs) removal. Three monophasic hybrid membranes were synthesized by combining phase inversion and sol-gel techniques: CA22-APT, CA22-APT-IBF(15%), and CA30-TEOS-APT-IBF(3%). Furthermore, it was developed four pure cellulose acetate membranes, CA22, CA30, CA33, and CA35, to evaluate the formamide influence through permeation studies.

All the membranes were characterized in the artificial kidney (AK) in terms of hydraulic permeability (Lp), permeation to PBUTs as well as HSA filtration. The molecular weight cut-off (MWCO) was accessed through the CELFA P-28 ultrafiltration installation. The morphological characterization was performed by Scanning Electron Microscopy (SEM), and the chemical composition was analyzed by Fourier Transform Infrared Spectroscopy in Attenuated Total Reflection mode (ATR-FTIR). Results for the CA30-TEOS-APT-IBF(3%) membrane showed a Lp of 97.6 $Kg \cdot h^{-1} \cdot m^{-2} \cdot bar^{-1}$, respectively. The MWCO for CA30-TEOS-APT-IBF(3%) showed a decrease in average pore sizes in comparison with the pure CA30 membrane. CA30-TEOS-APT-IBF(3%) membrane permeated IS and rejected 100% of HSA. Overall, the new membranes' performance is promising, and research should be continued to prove, for the first time, the permeation of PBUTs through competitive binding membranes.

Keywords: monophasic hybrid membranes; sol-gel; phase inversion; artificial kidney; competitive binding; blood purification

1 Introduction

The human kidney, among other things, is responsible for removing water, toxins, drugs, and waste products from the blood. Chronic Kidney Disease (CKD) is defined as abnormalities of kidney structure or inefficient removal of uremic toxins. It is characterized by an irreversible loss of renal function which can lead to End Stage Renal Disease (ESRD). Presently, there are only two options for the ESRD treatment: Renal Replacement Therapies (RRTs) or transplantation. However, there are some issues for both methods: transplantation is the most effective treatment but the scarcity of organ donors, the surgical risk of kidney transplantation, and the need for life-long immunosuppressive therapy greatly limit this option [1]. On the other hand, ESRD greatly limit the quality of life of ESRD patients as they require the visit to specialized clinics for more than four hours, three times a week – a routine procedure which must be maintained until transplantation or death.

The most widely used RRT is HD - an extracorporeal blood cleansing procedure used to eliminate metabolic waste products from patients with ESRD. The principle of HD involves the clearance of several solutes across a semipermeable membrane by diffusion and ultrafiltration processes, including the permeation of water excesses and several uremic toxins (UT) across the membrane, and retention of vital blood components such as albumin and blood cells. Different mass separation mechanisms are used to remove solutes and water through semipermeable membranes (diffusion, convection, and adsorption). In terms of structure, there are two main types of HD membranes: pure polymer membranes and Mixed Matrix Membranes (MMMs). Nevertheless, in recent years, another option for HD therapies has emerged: integral asymmetric monophasic hybrid membranes which will be discussed further in this study.

Uremic toxins can be classified in three main groups: i) Samll Water-Soluble Compounds (SWSC) (MW lower than 500 Da) such as urea, creatinine and uric acid; ii) middle molecules such as β_2-microglobulin (MW between 500 and 60000 Da); and iii) Protein-bound Uremic Toxins (PBUTs) (MW lower than 500 Da when free) as in case of Indoxyl Sulphate (IS) and p-Cresyl Sulfate (pCS) [1, 2]. The third group of toxins, PBUTs, are characterized as the main bottleneck to the efficient removal of all uremic toxins. The difficulty to remove PBUTs remains in the fact that these toxins exhibit high affinity with HSA (MW 66.4 kDa), a very large vital protein which cannot be removed in HD therapy. Approximately 90% of IS and pCS circulate in the blood bound to HSA while only 10% of these PBUTs circulate in their free form or unbound to HSA and only this small free fraction is dialyzable [3]. Due to the large size of the protein-toxin complex (MW higher than 66.4 kDa), PBUTs concentrations in the blood of ESRD patients who undergo HD remain essentially untouched. Since the two molecules, HSA and PBUTs, are linked by noncovalent bonds, the binding is reversible and follows the law of mass action, where the degree of binding is determined by the association and dissociation rate constants, among other things [4].

Albumin is one of the most essential and abundant proteins

in the blood, with a concentration of 35-50 mg/mL in human serum [5]. despite the strong affinity to PBUTs, HSA is responsible for transporting a variety of substances throughout the body, including enzymes, hormones, toxins, and pharmaceutical drugs. The literature shows that most compounds bind to 1 of 2 primary binding sites commonly referred to as Sudlow's binding sites I and II and IS, pCS, and IAA, bind to Sudlow's site II. In terms of binding between pharmaceutical drugs and HSA, warfarin is the prototypical ligand of Sudlow's site I, which is also known for binding other drugs like Furosemide (FUR), aspirin and benzylpenicillin. Sudlow's site II is known to be the binding site of diazepine, Tryptophan (TRP) and Ibuprofen (IBF) [1]. Several strategies to decrease the accumulation of PBUTs in the blood have been proposed by clinical researchers and scientists: i) maintenance of residual kidney function, ii) limitation of PBUTs generated in the colon, iii) administration of oral adsorbents, iv) use of adsorbent technology in current RRTs, v) membrane-based technology targeting the removal of PBUTs, and vi) infusion of HSA binding competitors [1]. The main focus of this work combines strategies v) and vi) and therefore will be discussed in detail.

The aim of this study is to develop novel HD membranes which target the removal of PBUTs by competitive binding. The proposal is to use pharmaceutical drugs as HSA displacers which will disrupt the PBUT-HSA structures to form new displacer-HSA complexes increasing the concentration of the free form of PBUTs. Higher concentrations of the free form of PBUTs are then removed by the novel HD membranes. Our approach is to functionalize monophasic hybrid cellulose acetate/silica (CA/SiO_2) membranes with IBF which will compete with PBUTs for the HSA binding site at the blood/membrane interface. It was synthesized four pure cellulose acetate membranes (CA22, CA30, CA33, and CA35) with different formamide percentage and three monophasic hybrid membranes (CA22-APT, CA22-APT-IBF(15%), and CA30-TEOS-APT-IBF(3%).

CA membranes exhibit poor mechanical strength, low chemical resistance, low thermal stability, sensitivity to cleaning agents, and vulnerability to fouling resistance, failing to achieve the desired separation/purification in some cases. The incorporation of different materials into the polymeric CA matrix, resulting in MMMs and hybrid membranes, may overcome some of the limitations of CA membranes. The formation of hybrid membranes involves the implementation of a novel monophasic material. One strategy is to select a coupling agent capable of promoting and maintaining an interconnected network.

The addition of silica and the subsequent formation of complex C-O-Si 3D networks is expected to improve membrane selectivity and permeation properties, as well as antifouling and mechanical stability, overcoming the limitations associated with pristine CA membranes. In hybrid monophasic SiO_2 membranes, the inorganic phase is dispersed and covalently bonded to the organic matrix. This type of membrane is synthesized in the casting solution homogenization phase by the co-condensation of SiO_2 alkoxysilane precursors during the sol-gel process [6, 7]. Thus, different silica precursors, such as TEOS and APTES and their derivatives, can be used to integrate SiO_2 into the polymer matrix by two processes: hydrolysis and condensation. Nitric acid is used to provide the acidic environment required to accelerate sol-gel hydrolysis and hetero-condensation processes.

2 Materials and Experimental Methods

2.1 Materials

Membranes were synthesized with CA ($C_6H_7O_2(OH)_3$, ~30 000 g/mol, reagent grade $\geq$ 97%, esterification degree 40%) and 3-(triethoxysilyl)-propylamine (APTES) ($C_9H_{23}NO_3Si$, 221.37 g/mol, reagent grade $\geq$ 98%) purchased from Sigma-Aldrich, tetraethyl orthosilicate (TEOS) ($Si(OC_2H_5)_4$, 208.33 g/mol, reagent grade 98%) purchased from Alfa Aesar, Formamide (CH_3NO, 45.02 g/mol, $\geq$ 99.5%) purchased from Carlo Erba, Acetone (C_3H_6O, 58.08 g/mol, $\geq$ 99.6%) and nitric acid (HNO_3, 63.01 g/mol, 1.39 g/mL at 20°C, 65% v/v) purchased from LabSolve, and IBF ($C_{13}H_{18}O_2$, 206.29 g/mol, racemic, reagent grade $\geq$ 98.0%) purchased from TCI.

Membranes drying was performed with isopropanol ($\geq$ 99.8%) from Honeywell and n-hexane ($\geq$95%) from Carlo Erba.

Permeation experiments were carried out with urea (MW 60.06 g/mol) purchased from Merck, creatinine (MW 113.12 g/mol) purchased from Sigma-Aldrich, uric acid (MW 168.11 g/mol) purchased from Alfa Aesar, IS (212 Da) purchased from Sigma-Aldrich, and Human plasma was obtained from healthy donors (IPO, Lisboa).

MWCO was studied using polyethylene glycol (PEG) 400 (MW 400 g/mol) purchased from Sigma-Aldrich, PEG 3000 (MW 3000 g/mol), PEG 6000 (MW 6000 g/mol), PEG 10000 (MW 10000 g/mol) purchased from Merck, PEG 20000 (MW 20000 g/mol) purchased from Sigma-Aldrich, PEG 35000 (MW 35000 g/mol) purchased from Merck, and dextran T40 (40 000 Da) purchased from Amersham Pharmacia Biotech AB.

Phosphate buffer saline was prepared using sodium chloride (NaCl, 58.44 g/mol, $\geq$ 99.5%) purchased from Merck, potassium chloride (KCl, 74.56 g/mol, $\geq$ 99.5%) purchased from Panreac, potassium dihydrogen phosphate (KH_2PO_4, 136.09 g/mol, $\geq$ 99.5%) purchased from Merck, and disodium hydrogen phosphate dihydrate ($Na_2HPO_4 \cdot 2\,H_2O$, 177.99 g/mol, $\geq$ 99.5%) purchased from Merck.

Quantification of HSA was carried out according to the Bradford protein assay. Bradford reagent was prepared using Coomassie Brilliant Blue G-250 ($C_{47}H_{48}N_3NaO_7S_2$, 854.04 g/mol) purchased from Panreac, ethanol (C_2H_6O, 46.07 g/mol, 96% v/v) purchased from Manuel Vieira, and phosphoric acid (H_3PO_4, 98.00 g/mol, 1.71 g/mL at 20°C, reagent grade 85%) purchased from Honeywell.

The compound APTES-IBF was synthesized using dicyclohexylcarbodiimide ($C_{13}H_{22}N_2$, 206.3 g/mol, reagent grade 99%) purchased from Thermo Fisher Scientific, 1-hydroxypyrrolidine-2,5-dione ($C_4H_5NO_3$, 115.09 g/mol) purchased from Sigma-Aldrich, and triethylamine ($(C_2H_5)_3N$, 101,19 g/mol, reagent grade $\geq$ 99.5%) purchased from Sigma-Aldrich.

2.2 Synthesis of SiO_2 precursors

The aim of this work is the incorporation of IBF into the active layer of the membranes with possible applications in HD.

For this purpose, the approach intended the conjugation of IBF into the membrane matrix through a covalent linkage to silica. The membrane synthesis precursors proved to be integrated in the polymer matrix [6]. The precursor IBF-APTES was linked to the CA matrix through the sol-gel reactions. It was synthesized two different membranes incorporating the precursor IBF-APTES: CA22-APT-IBF(15%) and CA30-TEOS-APT-IBF(3%).

2.2.1 Conjugation of ibuprofen (IBF) with (3-aminopropyl)triethoxysilane (APTES) (IBF-APTES)

In 5 mL of acetonitrile, APTES (53,6 mg, 0.242 mmol) was mixed with IBF (50,0 mg, 0.242 mmol). The mixture was treated with 99% dicyclohexylcarbodiimide (74,9 mg, 0,363 mmol), 1-hydroxypyrrolidine- 2,5-dione (41,8 mg, 0,363 mmol), and triethylamine (36,7 mg, 0,363 mmol) for 8 hours. After several washes with acetonitrile, the solvent was evaporated to dryness in a rotavapor, yielding a colourless oil. The mechanism for the APTES-IBF synthesis was detailed in previous studies [8].

2.3 Membrane Preparation

2.3.1 Pure Cellulose Acetate Membranes

CA membranes, CA22, CA30, CA33, CA35, were prepared through the phase inversion method from four casting solutions containing cellulose acetate, acetone and formamide with different formamide:acetone ratios. Table 1 shows the composition of the casting solutions.The membranes were then cast onto a glass plate (16 cm X 28 cm) at room temperature using a film casting knife with a thickness of 250 µm and after a solvent evaporation time of 30 seconds the glass plate was quenched into a gelation bath (ice-cold deionized water). After a residence time of approximately 24 h the membranes were detached from the glass plate, washed with deionized water (to remove any traces of solvent) and stored in deionized water at $4 \pm 1^{\circ}$ C.

Membrane	CA22	CA30	CA33	CA35
Cellulose Acetate (wt.%)	17	17	17	17
Formamide (wt.%)	22	30	33	35
Acetone (wt.%)	61	53	50	48

Table 1: Casting solution composition (wt.%) of the pure cellulose acetate (CA) membranes.

2.3.2 Monophasic Hybrid Membranes

The integral asymmetric monophasic hybrid CA/SiO_2 membranes, CA22-APT, CA22-APT-IBF(15%), CA30-TEOS-APT-IBF(3%), were formed adding to homogeneous casting solution composed by a solvent system (formamide and acetone) and CA, different TEOS and APTES ratios and nitric acid to promote the acidic hydrolysis. This solution will be stirred for 24 hours and then cast onto a glass plate (16 cm X 28 cm) at room temperature using a film casting knife with a thickness of 250 µm and after a solvent evaporation time of 30 seconds the glass plate was quenched into a gelation bath (ice-cold deionized water). After a residence time of approximately 24 h the membranes were detached from the glass plate, washed with deionized water (to remove any traces of solvent) and stored in deionized water at $4 \pm 1^{\circ}$ C.

Monophasic hybrid CA/SiO_2 membranes incorporating competitive binders were produced using the silica derivatives prepared and detailed previously. Since the competitive binder (ibuprofen) was conjugated with the silica precursors, when all of the other reagents (CA, acetone, and formamide) have been thoroughly mixed, the compound APTES-IBF is added to the casting solution and is incorporated through the sol-gel process. Following that, the phase inversion method is carried out as previously described. The percentage of IBF present in the name of the CA22-APT-IBF(15%) (15%) is only relative to the CA and APTES-IBF mass (do not include the formamide and acetone quantities). The same rationale was applied to the CA30-TEOS-APT-IBF(3%) membrane: 3% is relative to the quantity of CA, TEOS, and APTES-IBF.

Table 2 represents the composition of monophasic hybrid CA/SiO_2 membranes casting solutions. The CA22-APT membrane is labelled as (1), the CA22-APT-IBF(15%) membrane as (2) and the CA30-TEOS-APT-IBF(3%) membrane as (3).

Membrane	(1)	(2)	(3)
Cellulose Acetate (wt.%)	16.43	15.87	15.96
Formamide (wt.%)	21.26	20.54	28.20
Acetone (wt.%)	58.52	56.85	49.70
TEOS (wt.%)	-	-	4.85
APTES (wt.%)	3.78	-	-
HNO_3	3 drops*	3 drops*	3 drops*
APTES-IBF (wt.%)	-	6.74	1.29

*were not consider for the total mass

Table 2: Casting solution composition of the monophasic hybrid CA/SiO_2 membranes.

The sol-gel reactions that occur during the casting solution step of hybrid membranes have previously been described [9]. Following the sol-gel hydrolysis reactions, the silanol groups from the inorganic (TEOS) and hybrid (APTES) monomers hetero-condensate with the C-OH groups from the CA polymer, resulting in the formation of a new Si-O-C covalent bond. The sol-gel method was developed through acid catalysis. After that, the new hybrid casting solution is cast to form a monophasic hybrid membrane based on carbon, silica, and amine chemical species, resulting in complex carbon-silica networks.

2.4 Membrane Characterization

2.4.1 Membrane structure by Scanning Electron Microscopy

Prior to being imaged by scanning electron microscopy (SEM), all the synthesized membranes membranes were submitted to the drying process described by *Lui et al.* [10]. Samples of the dry membranes were broken in liquid nitrogen, mounted on a stub, and gold-sputtered prior to being analysed by SEM (Thermo Scientific Phenom ProX). The top dense surface of the membranes was analysed and images were taken at a magnification of 1000x, cross-sections were imaged at a magnification of 700x, 1800x, and 4200x and the porous bottom layer was

analysed and imaged at a magnification of 4000x. The software ImageJ (version 1.53t, from National Institutes of Health) was used to calculate the total and active layer thickness of the membranes on five different areas of each image of the cross-section of the membrane samples of each membrane, and the mean thickness and standard deviation were computed. The images were binarized using a threshold adjustment and then analysed using the Measure tool to calculate the average pore size of the porous bottom layer.

2.4.2 Membrane chemical composition by ATR-FTIR Spectroscopy

The chemical composition of the active layer surfaces of dried membrane samples was analysed by ATR-FTIR. The samples' infrared spectra were collected using a PerkinElmer Frontier FT-IR spectrometer (940 Winter Street, Waltham, MA 02451, USA), a Pike Miracle Single Reflection ATR sampling accessory from Pike Technologies, and a Ge crystal (Graseby Specac, Smyrna; sampling depth: 0.2-1.1 m at 4000-600 cm^{-1}). Averaging 256 images with a resolution of 4 cm^{-1} yielded each spectrum. The received infrared spectra were reported as percentage transmittance values as a function of wave number.

2.5 Membrane permeation performance

2.5.1 Artificial Kidney Experimental Setup

The permeation performance of the pure CA and monophasic hybrid membranes was determined in an experimental setup which simulates the pressure and flow conditions of a hemodialysis machine which is referred to in this thesis by the Artificial Kidney (AK) setup. Parameters, such as the hydraulic permeability (Lp), MWCO, permeation to SWSC and PBUTs, and long-term albumin filtration, were studied in a SHDMM to determine the mass transfer properties related with the metabolic functions of the kidney. Figure 1 shows the schematic representation of the AK experimental setup. The feed solution, stored in the feed reservoir, is circulated throughout the system by a peristaltic pump (ISM1079B, Pennsylvania, USA). A damper positioned before the first pressure sensor (P1) dampens the flow pulsations imposed by the peristaltic pump before entering the SHDMM. The feed solution is then returned to the feed reservoir with a second pressure sensor (P2) registers the pressure at the outlet of the SHDMM. The permeate (which crosses the membrane) is collected in a permeate reservoir after passing a third pressure sensor (P3). The medical grade pressure sensors (DPT-100, Westmeath, Ireland), capable of registering fluctuations as low as 1 mm Hg, are connected to a computer, where the Labview software registers the pressures every 2 seconds. The tubing where feed and permeate solutions are circulated is made of medical grade tygon (ND 100-65, Ohio, USA).

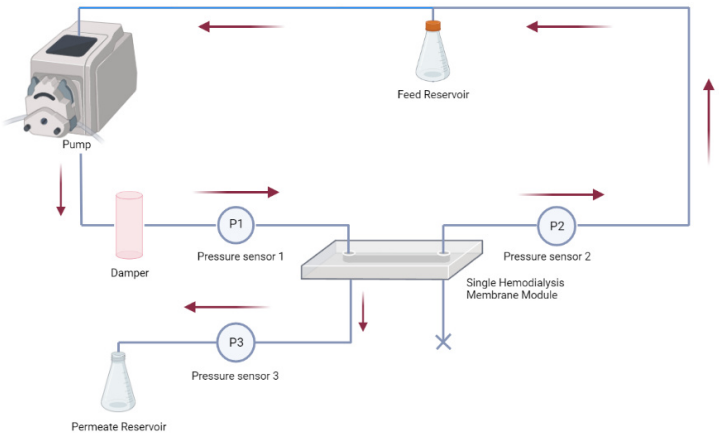

Figure 1: Experimental Setup for permeation studies.

The SHDMM which was designed by the Onshape software and printed on a 3D printer (Ultimaker 2^+, Gelderland, Netherlands). The membrane must be held in place by a spacer with a slit´geometry presenting an effective area of 4.76 cm^2 (middle piece). The height of the feed flow channel is an important parameter when assessing fouling events. The channel height (2B) may vary during permeation studies due to the deposition of molecules on top of the membrane. The dimensions of the feed and permeate microchannels are 2B = 0.3 cm, width (W) = 1.5 cm, and length (L) = 5 cm. Moreover, the total membrane surface area assumes the value of 7.5 cm^2.

Transmembrane Pressure (TMP) is determined as the average pressure in the blood compartment minus the average pressure in the dialysate compartment. It is defined as the hydrostatic pressure gradient that enables for ultrafiltration or convection through a dialyzer membrane [11]. In this case, TMP is given by Equation 1:

$$TMP = \frac{P1 + P2}{2} - P3 \tag{1}$$

Where P1, P2, and P3 are the pressure values of the different sensors.

The pressure drop (ΔP) given by Equation 2 is the difference in pressures between the input and output of the blood compartment from the membrane module.

$$\Delta P = P1 - P2 \tag{2}$$

The microchannel's half-height (B) is obtained by adjusting Equation 3, which is comparable to the Hagen-Poiseuille law for circular tubes and describes the fully-developed laminar flow of a Newtonian fluid in a narrow slit [12]:

$$B = \sqrt[3]{\frac{2}{3}\frac{\mu L}{W}\frac{Q_F}{\Delta P}} \tag{3}$$

Where Q_F is the volumetric feed flow rate collected by pump calibration curve, W and L is width and length of the spacer, μ is the viscosity of the fluid and Δ P is the pressure drop.

Shear stress (τ) is a fluid dynamics parameter that is essential for avoiding blood damage such as platelet activation and hemolysis. A healthy human vessel exhibits a shear stress of roughly 0.1 to 20 Pa: 0.1 to 1 Pa for veins and 1 to 20 Pa for arteries [13]. Platelet activation increases dramatically

when exposed to shear stress higher than 20 Pa and mechanical cell damage, hemolysis, at 30 Pa, according to previous studies [13, 14].

The shear stress at the flow boundaries, or microchannel walls, can be determined by balancing the shear force at the wall against the pressure gradient in a slit channel [12], as shown in Equation 4.

$$\tau = \frac{3\mu Q_F}{2B^2W} \tag{4}$$

Shear rates, γ, at the wall are determined by dividing shear stress by viscosity, as shown in Equation 5.

$$\gamma = \frac{\tau}{\mu} = \frac{3Q_F}{2B^2W} \tag{5}$$

2.5.2 Ultrafiltration experimental setup: CELFA P-28

The permeation performance of the membranes in terms of hydraulic permeability (Lp) and MWCO was also evaluated in a lab-scale crossflow ultrafiltration installation, Celfa P-28.

2.6 Permeation Studies

2.6.1 Hydraulic Permeability, Lp

The hydraulic permeability (Lp) describes the diffusive or convective transport through a membrane under the influence of a hydrostatic pressure driving force. Equation 6 describes the permeate water flux (J_w) which is defined as the amount of permeate produced per unit area of membrane surface per unit of time:

$$J_w = \frac{V}{A_{eff} \cdot t} = \frac{Q_{UF}}{A_{eff}} \tag{6}$$

where V is the volume of permeate, t is the measuring time, A_{eff} is the effective membrane filtration area, and Q_{UF} is the ultrafiltration flowrate measured.

When J_w is expressed as a function of TMP, a linear correlation is obtained and the Lp is determined from the slope of the straight line:

$$Lp = \frac{J_W}{TMP} \tag{7}$$

All experiments were made with deionized water at room temperature. Permeate is collected, weighed, and transformed in volume by water density and corrected for a temperature of 25ºC.

2.6.2 Molecular weight cut-off (MWCO)

A membrane's MWCO is defined as the lowest molecular weight (in Da) at which the membrane retains more than, 90% of a solute with a known molecular weight. A retention curve is constructed by measuring the rejection coefficient, R, to several PEGs with increasing molecular weights of 1000, 3000, 6000, 10 000, 20 000 and 35 000 Da, respectively. The rejection factor, f, defined by Equation 8, is characterized as the percentage of how much solute, initially in the feed solution, passes through the membrane to the permeate after a given time.

$$f = \frac{C_f - C_p}{C_f} \tag{8}$$

Where C_p corresponds to the solute concentration that was permeated by the membrane after a certain time and C_f corresponds to the initial feed solution concentration. Solute concentrations in the permeate and feed solutions were determined in triplicate using a Total Organic Carbon (TOC) analyzer (TOC-VCPH/CPN, Shimadzu, Japan). Thus, the MWCO is determined from the intersection of the linearized curve of $log(\frac{f}{1-f})$ as a function of MW and the MWCO value is provided by the intersection of the 90% rejection factor and the line connecting all rejection factors.

2.6.3 Permeation to Protein-bound uremic toxins (PBUTs)

200 mL of plasma spiked with 40 mg/L of Indoxyl Sulphate (IS), a surrogate marker for PBUTs, was recirculated through the SHDMM containing the CA30-TEOS-APT-IBF(3%) membranes in the AK setup for 8 hours at a feed rate of 100 mL/min and a TMP of 200 mmHg. Concentrations of IS were determined in samples taken from the permeate and feed solutions at different times of the experiment by fluorescence spectroscopy (fluorometer - FluoroJasco FP8500, Pfungstadt, Alemanha). The samples were excited at 275 nm and the emission spectra was collected from 300-500 nm at a scan speed of 200 nm/min using Xe as a light source.

2.6.4 Long-term HSA filtration

Permeation of HSA experiments were carried out using plasma collected from healthy patients in the AK experimental setup. 150-200 mL of plasma were circulated between 4 and 8 hours through the SHDMM containing the membranes CA30, CA30-TEOS-APT-IBF(3%), and CA35 at a feed rate of 100 mL/min and a TMP of 200 mmHg. Samples from the feed reservoir and permeate were collected every 60 minutes and HSA was quantified by the Bradford and modified Bradford methods, respectively. Specifically, the absorbance of feed samples was measured at 595 nm, following the Bradford assay [15], whereas the absorbance of permeate samples was simultaneously measured at 590 nm and 450 nm according to a modified Bradford assay [16], allowing the determination of lower BSA concentrations. UV spectrophotometry is used for detection.

3 Results

3.1 Membrane Characterization

3.1.1 Membrane structure by Scanning Electron Microscopy

Figure 2 represents the cross section of the (a) CA22 and (b) CA22-APT-IBF(15%) membranes. From these images it is possible to confirm the integral asymmetric structure with a very thin dense active layer and a much thicker, porous substructure.

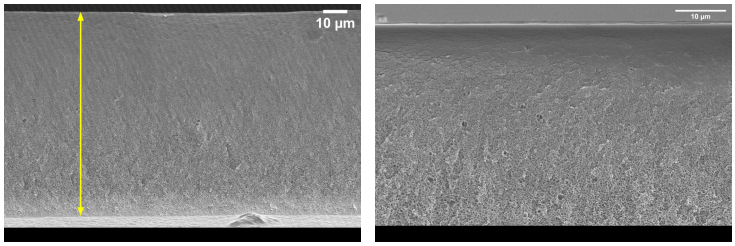

(a) (b)

Figure 2: SEM images: cross section imaged at a magnification of 860x and 1800x for (a) CA22 and (b) CA22-APT-IBF(15%) membranes.

Table 3 represents the overall membrane thickness of the membranes which was obtained from the cross-section images. For the CA22, CA22-APT, CA22-APT-IBF(15%), CA30, CA30-TEOS-APT-IBF(3%), CA33, and CA35 membranes were obtained a thickness of 83.8 ± 0.39, 101.3 ± 0.74, 95.3 ± 1.56, 77.3 ± 0.53, 83.4 ± 1.13, 96.2 ± 0.19, 88.6 ± 0.65 µm, respectively. Analyzing the thickness of the pure cellulose acetate membranes (CA22, CA30, CA33, and CA35), it is possible to conclude that the CA33 membrane has the highest membrane thickness (96.2 ± 0.19 µm)), while the CA30 has the lowest (77.3 ± 0.53 µm)). However, due to the formamide content, CA35 membrane was expected to be the thickest, while CA22 membrane would be the thinnest.

Membrane	Thickness (µm)
CA22	83.8 ± 0.39
CA22-APT	101.3 ± 0.74
CA22-APT-IBF(15%)	95.3 ± 1.56
CA30	77.3 ± 0.53
CA30-TEOS-APT-IBF(3%)	83.4 ± 1.13
CA33	96.2 ± 0.19
CA35	88.6 ± 0.65

Table 3: Mean membrane thickness and standard deviation for the cross-section images calculated by the ImageJ image analysis programme.

3.2 Membrane chemical composition by ATR-FTIR Spectroscopy

The ATR-FTIR spectra of the CA22, CA30, CA33, and CA35 membranes are compared in Figure 3. The broad band centred at approximately 3478 cm^{-1} is assigned to the OH stretching mode, ν(OH), and contains contributions from non-esterified cellulose hydroxyl groups as well as silanol groups.

Identically to previous work [6], the strong carbonyl stretching mode, ν(C=O), appears at 1742 cm^{-1}, while the anti-symmetric, ν_{as}(C-O-C), and symmetric, ν_s(C-O-C) stretching modes of the ester appear as strong bands at 1228 cm^{-1} and 1040 cm^{-1}, respectively. Moreover, the band centered at 1370 cm^{-1} is assigned to δCH_3 [9]. The weak band centered at 904 cm^{-1} confirms the presence of acetate methyl groups [9].

All the pure cellulose acetate membranes studied, CA22, CA30, CA33, and CA35 present the same ATR-FTIR spectra, as expected.

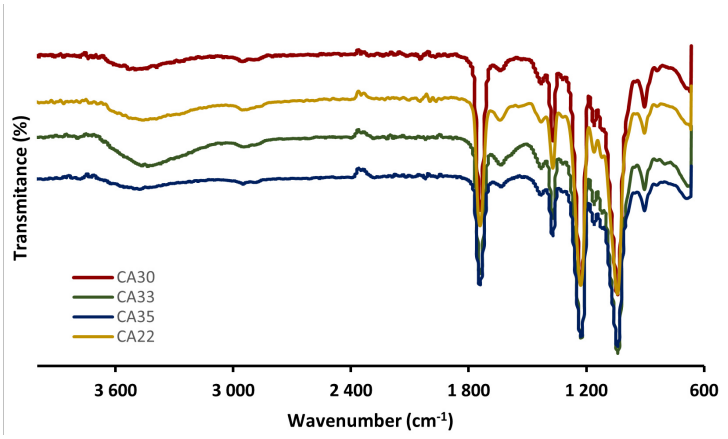

Figure 3: Wide-range ATR-FTIR spectra (4000-600 cm^{-1}) of the CA22, CA30, CA33, and CA35 membranes.

Figure 4 represents the comparison between the ATR-FTIR spectra of the CA22, CA22-APT-IBF(15%) membranes with the ATR-FTIR spectra of IBF. The literature [17] shows that for a characteristic vibration frequency of 3095 cm^{-1} and between 1579 and 1408 cm^{-1}, there are located the aromatic C-H and C=C stretching, respectively. From the data observation, it is possible to observe these peaks in the ATR-FTIR spectra of IBF, however for the CA22-APT-IBF(15%) membrane, these bands are not visible. This observation can be attributed to a variety of factors: the superposition of the characteristic peaks or the very low amount of IBF in the membrane composition.

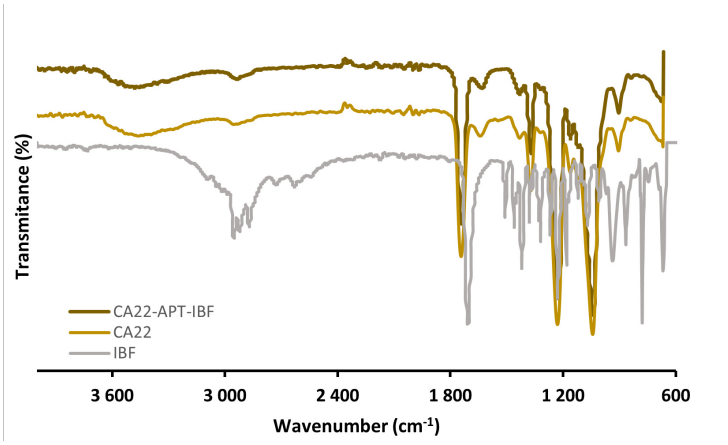

Figure 4: Wide-range ATR-FTIR spectra (4000-600 cm^{-1}) of IBF, CA22 and CA22-APT-IBF(15%) membranes.

Figure 5 depicts the ATR-FTIR spectrum of the CA30 and CA30-TEOS-APT-IBF(3%) membranes, as well as the binding competitor IBF. Once again, several vibration bands of the IBF spectra do not appear in the ATR-FTIR spectrum of the CA30-TEOS-APT-IBF(3%) membrane. These results can be attributed to the membrane's lower IBF content. For future analysis, the ATR-FTIR spectra of the precursor APTES-IBF should also be included.

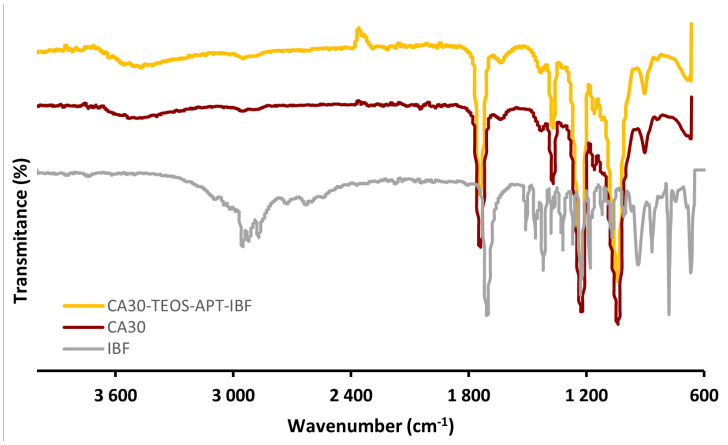

Figure 5: Wide-range ATR-FTIR spectra (4000-600 cm^{-1}) of IBF, CA30 and CA30-TEOS-APT-IBF(3%) membranes.

3.3 Pressure drop, microchannel height, shear rate and shear stress at the wall

Table 4 contains the microchannel height (2B) results obtained for the SHDMM when containing the CA30, CA30-TEOS-APT-IBF(3%), CA33, and CA35 membranes. The height of the channel when no membrane is present is 300 μm but when a membrane is placed inside the SHDMM this value will change. According to the data, for the CA30, and CA30-TEOS-APT-IBF(3%) membranes the value of 2B is identical (260 and 258 µm, respectively). On the other hand, the CA33, and CA35 membranes also present a very similar 2B, being 229 µm for the CA33 and 226 µm for the CA35 membrane. In addition, the differences observed can be related to the composition of the membranes: the CA33 and CA35 membranes contain a higher percentage of formamide than the CA30 and CA30-TEOS-APT-IBF(3%) membranes, and thus are thicker, as confirmed by SEM, resulting in a decrease in 2B for these membranes. Both the CA30 and CA30-TEOS-APT-IBF(3%) membranes contain 30% formamide, so the 2B is nearly the same.

	CA30	CA30-TEOS-APT-IBF(3%)	CA33	CA35
2B (µm)	260	258	229	225

Table 4: Microchannel´s height (µm) for the CA22, CA30, CA30-TEOS-APT-IBF(3%), CA33, and CA35 membranes at Q_F = 100 mL/min. Experiments were carried out with ultra-pure water.

The data reported in Table 5 contains the shear stress (τ), shear rate (γ), and ΔP obtained for the CA30, CA30-TEOS-APT-IBF(3%), CA33, and CA35 membranes. The experiments were performed with ultra-pure water at 25°C in the AK setup at a feed flow rate (Q_F) of 100 mL/min and for TMPs ranging from 125 – 135 mmHg. Furthermore, the shear stress assumed very similar values for all of the membranes studied, ranging from 9.9 to 12.0 Pa, with the CA30 exhibiting the lowest value. The shear rate is also very similar for all the membranes ranging from $1.11{\cdot}10^4$ to $1.36{\cdot}10^4$ s^{-1} as well as the ΔP which vary from 26.0 to 39.7 mmHg. These results are consistent with expectations; it is implied that these parameters do not vary depending on the membrane used since they are mainly determined by the feed flow rate, fluid viscosity, and SHDMM dimensions. However, it is important to confirm that these values are within the normal range for each membrane and assay.

	CA30	CA30-TEOS-APT-IBF(3%)	CA33	CA35
τ (Pa)	9.90	12.0	11.6	11.9
γ (s^{-1})	$1.11 \cdot 10^4$	$1.35 \cdot 10^4$	$1.30 \cdot 10^4$	$1.36 \cdot 10^4$
ΔP (mmHg)	26.0	34.9	38.1	39.7

Table 5: Shear stress (Pa), shear rate (s^{-1}), and ΔP (mmHg) obtained at 25°C for the CA22, CA30, CA30-TEOS-APT-IBF(3%), CA33, and CA35 membranes at Q_F = 100 mL/min. Experiments were carried out with ultra-pure water.

3.4 Permeation Studies

3.4.1 Hydraulic Permeability, Lp

Figure 6 represents the $Lp^{25°C}$ for the CA22, CA22-APT and CA22-APT-IBF(15%) performed in CELFA P-28. It was obtained a $Lp^{25°C}$ of 24.0, 8.7, and 1.0 $Kg \cdot h^{-1} \cdot m^{-2} \cdot bar^{-1}$ for the CA22, CA22-APT, and CA22-APT-IBF(15%) membranes, respectively. All of these membranes contain the same formamide content; CA22-APT and CA22-APT-IBF(15%) have APTES in their composition as a silica precursor and CA22-APT-IBF(15%) present the binding competitor linked to APTES. It can be seen that the lowest $Lp^{25°C}$ was achieved for the CA22-APT-IBF membrane while for the CA22 and CA22-APT, the $Lp^{25°C}$ present a lower Lp value. The very low Lp values for the CA22-APT and CA22-APT-IBF (15%) can be attributed to the presence of several macroporous structures in both membranes that difficult the passage of water and thus, result in very low ultrafiltration fluxes.

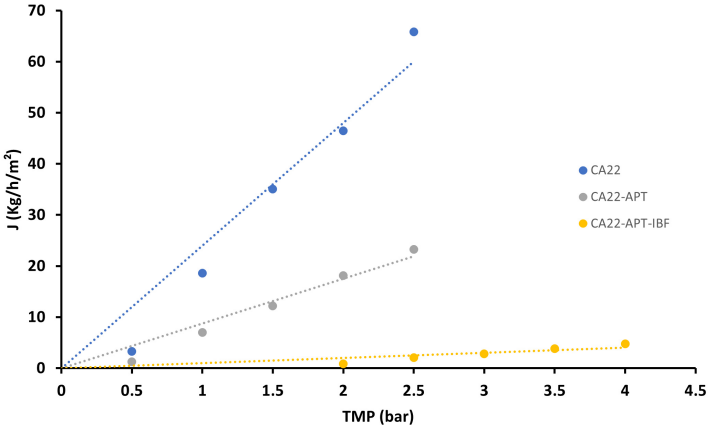

Figure 6: Ultrafiltration flux at 25°C, $J^{25°C}$, in $Kg/h/m^2$, as a function of the applied transmembrane pressure (TMP), in bar, for the CA22, CA22-APT, and CA22-APT8IBF) membranes measured in CELFA P-28. The ultrafiltration fluxes were measured at a volumetric feed flow rate of 9.80 $cm^3 \cdot s^{-1}$ and with an effective area of 15 cm^2.

Figure 7 depicts the $Lp^{25°C}$ of CA30 and CA30-TEOS-APT(3%) membranes. The $Lp^{25°C}$ is 68.6 $Kg{\cdot}h^{-1}{\cdot}m^{-2}{\cdot}bar^{-1}$ for the CA30 membrane while for the CA30-TEOS-APT(3%) membranes is 97.6 $Kg \cdot h^{-1} \cdot m^{-2} \cdot bar^{-1}$. Both membranes have the same amount of formamide; CA30-TEOS-APT(3%) is

a hybrid monophasic membrane that has TEOS and APTES as silica precursors and IBF linked to APTES. It can be seen that the $Lp^{25^\circ C}$ of CA30-TEOS-APT(3%) membrane is higher than the $Lp^{25^\circ C}$ of the CA30 membrane. In contrast to the previous membranes with 22% formamide, the monophasic hybrid membrane here has a higher Lp than the pure cellulose acetate membrane. Previously, it was reported [8] a different behavior for these two membranes where their $Lp^{25^\circ C}$ value is very similar (37.50 $Kg \cdot h^{-1} \cdot m^{-2} \cdot bar^{-1}$ for CA30 and 35.90 $Kg \cdot h^{-1} \cdot m^{-2} \cdot bar^{-1}$ for CA30-TEOS-APT-IBF(3%).

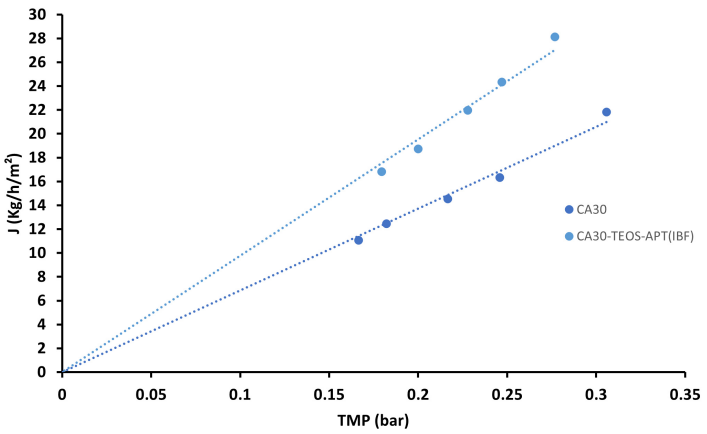

Figure 7: Ultrafiltration flux at $25^\circ C$, $J^{25^\circ C}$, in $Kg/h/m^2$, as a function of the applied transmembrane pressure (TMP), in bar, for the CA30, and CA30-TEOS-APT(IBF) membranes measured in the AK setup. The ultrafiltration fluxes were measured at a volumetric feed flow rate of 100 mL/min and with an effective area of 4.76 cm^2.

Throughout the analysis of the results, it can be seen that the presence of silica precursors functionalized with IBF affects the hydraulic permeability of the membranes. However, it can be obtained different conclusions according to different membranes.

3.4.2 Molecular weight cut-off (MWCO)

The MWCO of the CA22, CA30, CA30-TEOS-ATP-IBF(3%), and CA35 was determined from the apparent rejection coefficients to PEGs of increasing molecular weights. Table 6 depicts the determined values of MWCOs for the CA22, CA30, CA30-TEOS-APT-IBF(3%) membranes where the MWCO range presented for each membrane corresponds to the intersection point of the plotted rejection coefficient curve ($MWCO_1$) and subsequent linearization ($MWCO_2$) with the respective horizontal rejection line.

Membrane	MWCO range (kDa)
CA22	6.6 - 7.7
CA30	32.9 - 36.6
CA30-TEOS-APT-IBF(3%)	18.9 - 23.2
CA35	39.2 - 39.8

Table 6: MWCO range, in Da, of the CA22, CA30, CA30-TEOS-APT-IBF(3%), and CA35 membranes.

Because formamide is responsible for the formation of pores in the membrane, the membrane with a lower formamide percentage is expected to have a lower MWCO. Therefore, results show that, as expected, the MWCO of the pure cellulose acetate membranes increases with the increase of formamide concentration in the casting solution. Hence, the MWCO increased from 6.6-7.7 kDa for the CA22 membrane to 39.2-39.8 kDa for the CA35 membrane and the CA30 membrane exhibits an intermediate MWCO value of 32.9 – 36.6 kDa.

Janeca et al. [11] reported a MWCO of the CA30 membrane between 17.6 and 18.6 kDa which is slightly below the value obtained for the CA30 membrane in this study. The results do not follow the same order as was seen for the Lp. From the $Lp^{25^\circ C}$ results of the AK setup, it can be observed that the membrane with the highest hydraulic permeability (CA30-TEOS-APT-IBF(3%)) does not exhibit the highest MWCO. Comparing the MWCO of CA30, and CA30-TEOS-APT-IBF(3%) it can be observed that the introduction of the TEOS-APT-IBF precursor into the polymer matrix decreased the MWCO from 32.9 – 36.6 kDa to 18.9 – 23.3 kDa. *Janeca et al.* [11] also reported another membrane with 30% of formamide which incorporated APTES as a silica precursor and for this membrane the MWCO assumed a value between 22.2 and 26.7 kDa which is also very similar to the one obtained for the CA30-TEOS-APT-IBF-(3%) membrane.

It is important to reinforce that membranes are from different batches and it is normal that there exists some variations in the membrane structure and thus in the MWCO. The evaporation time of the solvent and the conditions of the casting solution can also influence the membrane structure.

Since all membranes reject solutes with MWs greater than 40 kDa, it is predicted that vital blood components such as albumin and other proteins, which have MWs larger than 60 kDa, will be successfully retained by the membranes. In addition, because they can cross the membrane, molecules belonging to two different classes of uremic toxins - small water-soluble compounds and middle molecules - are expected to be able to cross the membranes and ultimately be removed from the blood.

3.5 Permeation to Protein-bound uremic toxins (PBUTs)

The permeation to PBUTs was performed with CA30-TEOS-APT-IBF(3%) membrane, after incubating the plasma with IS, a IS free percentage of 2.03 ± 0.04 and 2.02 ± 0.11 % was obtained at the beginning (T = 0 min) and at the end (T = 390 min) of the experiment, respectively. These result are consistent with previous studies in which 98% of the total concentration of IS binds to HSA [3]. According to the results, the total concentration of IS at the end of the experiment (52.3 mg/L) was higher than the real concentration used (40.0 mg/L), being an incoherent result. In addition, the total form of IS decreased from 4838.7 to 4807.6 µg during the experiment, suggesting that 31.1 µg of IS were permeated by the membrane. On the other hand, the IS free form decreased only 1.4 µg throughout the experiment.

Table 7 contains the data obtained regarding the IS removal thought the CA30-TEOS-APT-IBF(3%) membrane. Throughout the observations of these results it can be concluded that: 1) IS was reported in the permeate, and its removal is constant throughout the test - except for the first half hour, the perme-

ate concentration was always around 1 mg/L; 2) At the end of the assay, 31.1 µg of IS were removed from the feed solution; 3) When compared to the IS concentration in the feed solution (40 mg/L), the concentration of IS permeated was very low (1 mg/L); 4) The free form of IS (98.4 µg) in the feed solution was not totally permeated by the CA30-TEOS-APT-IBF(3%) membrane.

Aside from that, the IS quantification in the feed solution suggests that 31.1 µg has been removed during the experiment. In addition, IS quantification in the permeate (Table 7) reveals that the CA30-TEOS-APT-IBF(3%) membrane effectively permeated 31.1 µg and thus, demonstrating that both quantification's, in feed and permeate solutions, are consistent. Furthermore, because the free portion of IS decreased only 1.40 µg in the feed solution while 31.1 µg of IS was quantified in the permeate, this finding may indicate that IS from the bound part may dissociate from the HSA during the experiment and become free in the solution and thus, able to be permeated. Nonetheless, there is the possibility of HSA-IS dissociation during the experiment, and these results must be confirmed.

Time (min)	[IS] mg/L	IS mass (µg)
0	0	0
30	0.07	0.20
90	1.03	6.16
150	0.99	5.60
210	1.00	5.19
270	0.99	4.80
330	0.96	4.30
390	1.13	4.81

Table 7: Data of IS permeation through the CA30-TEOS-APT-IBF(3%) membrane.

A higher effective area of permeation is necessary to permeate all of the free IS present in the feed solution. Thought the results obtained, cannot be determine whether the IS permeated by the CA30-TEOS-APTES-IBF(3%) membrane corresponds to the free or bound portion. The effect of the binding competitor IBF can be detected by higher permeation rates or by a significantly decrease in the free form of IS in the feed solution. Moreover, the HSA-IS association/dissociation rates during the experiment must be further investigated.

3.5.1 Long-term HSA filtration

Figure 8 represents the concentration profiles of HSA as well as the pressure profiles (TMP and ΔP) during long term HSA filtration experiments performed in the AK setup with the CA30-TEOS-APT-IBF(3%) membrane.

The results showed that the highest HSA concentration detected in the permeate samples was 4.6 mg/L. Taking into account that the initial concentration of HSA ranging between 40 000 to 50 000 mg/L, the rejection factor to albumin for each membrane was 100%.

It can be observed that there is some variations in the TMP as well as ΔP over time: the TMP increased from 250 mmHg to 290 mmHg during the assay; the ΔP also assumed some variations over time, oscillating between 30 to 45 mmHg. As a result, these pressure differences may indicate some deposition and accumulation of unwanted components at the membrane's surface. Therefore, it can be an indicator that albumin linked to IBF present at the surface of the membrane, resulting in their deposition increasing the pressure, consequently. Nevertheless, fluid removal over time, which leads to an increase in protein concentration and, as a result, an increase in plasma viscosity, can also justify these observations.

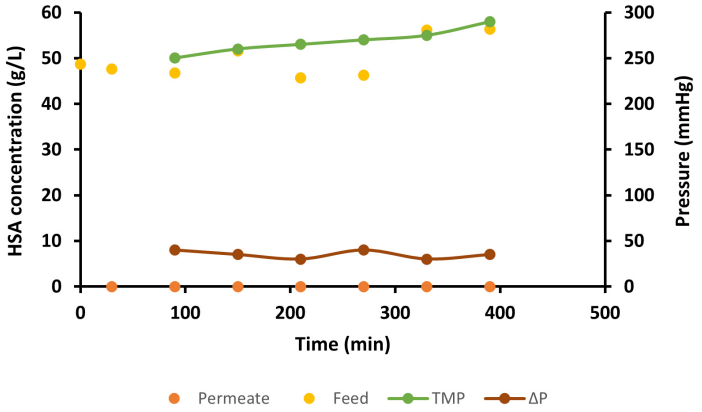

Figure 8: HSA concentration and pressure profiles (g/L) for (b) CA30-TEOS-APT-IBF, regarding feed (yellow) and permeate (orange) samples along the time (min).

As mentioned previously, for the CA30-TEOS-APT-IBF(3%) membranes, it was obtained a rejection coefficient of 100%. These findings are consistent with the predictions due to the MW of HSA, and the MWCO of each membrane which is below 40 kDa. Moreover, CA30-TEOS-APT-IBF(3%) membrane shows promising results in terms of inhibiting albumin leakage, which is highly undesirable in a clinical scenario, during HD sessions.

4 Conclusion

PBUTs are regarded as the main bottleneck to the efficient removal of all uremic toxins and are associated with a variety of Chronic Kidney Disease (CKD) complications. The infusion of HSA binding competitors into the bloodstreams of End Stage Renal Disease (ESRD) patients opened a new research pathway for the removal of PBUTs. However, the side effects of long-term administration of large amounts of pharmaceutical drugs into ESRD patients' bloodstreams highlight the need for another alternative.

This work proved the synthesis of integral asymmetric, hybrid monophasic cellulose acetate/silica with the incorporation of IBF as a binding competitor. The novel CA30-TEOS-APT-IBF(3%) membrane showed a hydraulic permeability similar than pure cellulose acetate membranes and successfully permeated IS and rejected 100% of HSA.

Future studies could address the reproduction of permeation experiments with indoxyl sulphate (IS); it is essential to carry out experiments in the AK setup with blood to evaluate shear rate and shear stress at the walls; evaluate the permeation of competitive binding membranes to small water-soluble compounds; use a larger effective area of membrane; perform a leaching assay to evaluate the binding of IBF to the mem-

brane; and use a higher content of the compound APTES-IBF to better evaluate their effect in the membrane performance.

5 Acknowledgements

This document was written and made publically available as an institutional academic requirement and as a part of the evaluation of the MSc thesis in Bioengineering and Nanosystems of the author at Instituto Superior Técnico. The work described herein was performed at the Center of Physics and Engineering of Advanced Materials of Instituto Superior Tecnico (Lisbon, Portugal), during the period March-October 2022, under the supervision of Monica Cristina Faria Besteiro and Maria Clara Henriques Baptista Gonçalves.

References

[1] M. Faria and M. N. de Pinho, "Challenges of reducing protein-bound uremic toxin levels in chronic kidney disease and end stage renal disease," *Translational Research*, vol. 229, pp. 115–134, 2021, DOI: https://doi.org/10.1016/j.trsl.2020.09.001.

[2] E. Sánchez-Álvarez, M. Rodríguez-García, F. Locatelli, C. Zoccali, A. Martín-Malo, J. Floege, M. Ketteler, G. London, J. L. Górriz, B. Rutkowski *et al.*, "Survival with low-and high-flux dialysis," *Clinical kidney journal*, vol. 14, no. 8, pp. 1915–1923, 2021, DOI: https://doi.org/10.1093/ckj/sfaa233.

[3] Y. Itoh, A. Ezawa, K. Kikuchi, Y. Tsuruta, and T. Niwa, "Protein-bound uremic toxins in hemodialysis patients measured by liquid chromatography/tandem mass spectrometry and their effects on endothelial ROS production," *Analytical and Bioanalytical Chemistry*, vol. 403, no. 7, pp. 1841–1850, 2012.

[4] L. Sultatos, "Drug reservoirs," *xPharm: The Comprehensive Pharmacology Reference*, pp. 1–2, 2007.

[5] T. Peters Jr, *All about albumin: biochemistry, genetics, and medical applications*. Academic press, 1995.

[6] G. Mendes, M. Faria, A. Carvalho, M. C. Gonçalves, and M. N. de Pinho, "Structure of water in hybrid cellulose acetate-silica ultrafiltration membranes and permeation properties," *Carbohydrate Polymers*, vol. 189, pp. 342–351, 2018. [Online]. Available: http://dx.doi.org/10.1016/j.carbpol.2018.02.030

[7] C.J. Brinker; G. W. Scherer, "Sol-Gel Science The physics and chemistry of sol-gel processing - Brinker 1990.pdf," p. 462, 1990.

[8] M. Lopes, "Towards nanostructured membranes for the artificial kidney," MSc Dissertation, Instituto Superior Técnico, Lisboa, 2021.

[9] M. C. Andrade, J. C. Pereira, N. de Almeida, P. Marques, M. Faria, and M. C. Gonçalves, "Improving hydraulic permeability, mechanical properties, and chemical functionality of cellulose acetate-based membranes by co-polymerization with tetraethyl orthosilicate and 3-(aminopropyl)triethoxysilane," *Carbohydrate Polymers*, vol. 261, no. November 2020, 2021, DOI: https://doi.org/10.1016/j.carbpol.2021.117813.

[10] A. Lui, F. Talbot, A. Fouda, T. Matsuura, and S. Sourirajan, "Studies on the solvent exchange technique for making dry cellulose acetate membranes for the separation of gaseous mixtures," *Journal of applied polymer science*, vol. 36, no. 8, pp. 1809–1820, 1988, DOI: https://doi.org/10.1002/app.1988.070360808.

[11] A. Janeca, F. S. Rodrigues, M. C. Gonçalves, and M. Faria, "Novel cellulose acetate-based monophasic hybrid membranes for improved blood purification devices: Characterization under dynamic conditions," *Membranes*, vol. 11, no. 11, 2021, DOI: https://doi.org/10.3390/membranes11110825.

[12] V. S. Vaidhyanathan, *Transport phenomena*, 1980, vol. 36, no. 11.

[13] S. S. Lee, K. H. Ahn, S. J. Lee, K. Sun, P. T. Goedhart, and M. R. Hardeman, "Shear induced damage of red blood cells monitored by the decrease of their deformability," *Korea-Australia Rheology Journal*, vol. 16, no. 3, pp. 141–146, 2004.

[14] Q. Lu, B. V. Hofferbert, G. Koo, and R. A. Malinauskas, "In vitro shear stress-induced platelet activation: Sensitivity of human and bovine blood," *Artificial Organs*, vol. 37, no. 10, pp. 894–903, 2013, DOI: https://doi.org/10.1111/aor.12099.

[15] M. M. Bradford, "A rapid and sensitive method for the quantitation of microgram quantities of protein utilizing the principle of protein-dye binding." *Analytical biochemistry*, vol. 72, pp. 248–54, 1976, DOI: https://doi.org/10.1016/0003-2697(76)90527-3.

[16] T. Zor and Z. Selinger, "Linearization of the bradford protein assay increases its sensitivity: Theoretical and experimental studies," *Analytical Biochemistry*, vol. 236, no. 2, pp. 302–308, 1996, DOI: https://doi.org/10.1006/abio.1996.0171.

[17] M. R. Pereira and J. Yarwood, "ATR-FTIR spectroscopic studies of the structure and permeability of sulfonated poly(ether sulfone) membranes Part 2. - Water diffusion processes," *Journal of the Chemical Society - Faraday Transactions*, vol. 92, no. 15, pp. 2737–2743, 1996.